Check for updates

Transdermal on-demand drug delivery based on an iontophoretic hollow microneedle array system†

Usanee Detamornrat, [iD] ‡[a] Marc Parrilla, [iD] ‡*[abc] Juan Domínguez-Robles,[a] Qonita Kurnia Anjani,[a] Eneko Larrañeta,[a] Karolien De Wael [iD] [bc] and Ryan F. Donnelly [iD] *[a]

Transdermal drug delivery has emerged as an alternative administration route for therapeutic drugs, overcoming current issues in oral and parenteral administration. However, this technology is hindered by the low permeability of the *stratum corneum* of the skin. In this work, we develop a synergic combination of two enhancing technologies to contribute to an improved and on-demand drug delivery through an iontophoretic system coupled with hollow microneedles (HMNs). For the first time, a polymeric HMN array coupled with integrated iontophoresis for the delivery of charged molecules and macromolecules (*e.g.* proteins) is devised. To prove the concept, methylene blue, fluorescein sodium, lidocaine hydrochloride, and bovine serum albumin–fluorescein isothiocyanate conjugate (BSA-FITC) were first tested in an *in vitro* setup using 1.5% agarose gel model. Subsequently, the *ex vivo* drug permeation study using a Franz diffusion cell was conducted, exhibiting a 61-fold, 43-fold, 54-fold, and 17-fold increment of the permeation of methylene blue, fluorescein sodium, lidocaine hydrochloride, and BSA-FITC, respectively, during the application of 1 mA cm^{-2} current for 6 h. Moreover, the total amount of drug delivered (*i.e.* in the skin and receptor compartment) was analysed to untangle the different delivery profiles according to the types of molecule. Finally, the integration of the anode and cathode into an iontophoretic hollow microneedle array system (IHMAS) offers the full miniaturisation of the concept. Overall, the IHMAS device provides a versatile wearable technology for transdermal on-demand drug delivery that can improve the administration of personalised doses, and potentially enhance precision medicine.

Introduction

Transdermal drug delivery has become an attractive and valuable administration route, overcoming certain limitations offered by traditional oral or parenteral routes.[1,2] Transdermal drug delivery avoids drawbacks such as poor drug stability in the gastrointestinal tract exhibited during oral intake, as well as circumvents the painful procedures required for the parenteral drug administration. However, the permeation of molecules *via* transdermal drug delivery is limited by the *stratum corneum* of the skin. In general, transdermal drug delivery has been used for certain molecules (*e.g.* molecular weight < 500 Da, adequate lipophilicity, and low melting point).[3] The permeation of large molecules (>500 Da) is typically restricted by the *stratum corneum*; hence additional technologies or drug carriers are needed to enhance their permeation. Traditionally, iontophoresis coupled with transdermal patches has been used to increase drug permeation through the skin and allow the delivery of drugs through hair follicles and sweat glands.[4,5] Furthermore, iontophoresis offers the ability to control delivery rates in real-time, thus augmenting the capabilities of transdermal drug delivery.[1,5,6] However, transdermal iontophoresis also presents some limitations, including low efficiency in drug delivery, the size exclusion of drugs larger than 12 kDa limiting its delivery, and the potential for skin irritation.[5] Consequently, the integration of iontophoresis with new technologies is pursued to mitigate these limitations and enhance drug permeation across the skin[3,7] as well as in other tissues and organs.[8] Enhancing

[a] *School of Pharmacy, Medical Biology Centre, Queen's University Belfast, 97 Lisburn Road, Belfast BT9 7BL, UK. E-mail: r.donnelly@qub.ac.uk*
[b] *A-Sense Lab, Department of Bioscience Engineering, University of Antwerp, Groenenborgerlaan 171, 2020 Antwerp, Belgium. E-mail: marc.parrillapons@uantwerpen.be*
[c] *NANOlab Center of Excellence, University of Antwerp, Groenenborgerlaan 171, 2020, Antwerp, Belgium*
† Electronic supplementary information (ESI) available: Details of the HMN array characterisation, fabrication of the holder, dimensions and pictures of the setup. See DOI: https://doi.org/10.1039/d3lc00160a
‡ Shared authorship.

technologies such as sonophoresis,[9] the employment of chemical penetration enhancers,[10] microneedles (MNs)[11] or a combination of them[12] have proven an excellent synergy with iontophoresis for the on-demand delivery of the different types of drugs, from small molecules to macromolecules.

MNs are minimally invasive devices that have been exploited mainly for passive drug delivery. By disrupting the outer layer of the skin, the *stratum corneum*, and creating hydrophilic microchannels, the diffusion of drug cargo from the MNs to either the epidermis or dermis layers can occur.[13] Depending on the dimensions, MNs can be designed to reach the lower layers of the skin (*e.g.* dermis) and deliver drug(s) in the interstitial fluid (ISF), allowing a systemic administration by the proximity of capillary blood vessels.[14] Several types of MNs, including hydrogel-forming MNs,[15] dissolving MNs,[16] hollow MNs (HMNs),[17,18] coated MNs,[19] and porous MNs,[20] have been employed for transdermal drug delivery. On the other hand, MNs have also been used for diagnosis purposes due to their minimally-invasive nature and the ability to monitor analytes in ISF.[21,22] Several strategies have been designed to *in situ* detect the target of interest, with electrochemical sensors, a widely used approach.[23] These strategies include: (i) the use of a solid MN patch as an electrode,[24,25] (ii) the embodiment of the electrode inside a HMN,[26,27] or (iii) the employment of a HMN patch to extract ISF toward a microfluidic cell for proper analysis.[28]

Stimuli-responsive MN patches represent an emerging delivery technology that releases cargo on-demand in response to internal or external triggers, such as thermal, photo, electrical, mechanical, pH-based, or enzymatic stimuli.[29] Electrical stimulation is particularly appealing, as it allows to control drug administration through a digital interface, enabling the maintenance of a desired therapeutic level. Recently, self-powered electrical stimuli drug delivery systems are becoming highly relevant as these systems can provide enhanced and/or on-demand delivery without the necessity of an external power source.[30] Electrical stimuli can be provided by: (i) an iontophoretic system,[31] or (ii) conductive polymers whose oxidation triggers the release of the drug.[32,33] However, the latter strategy deals with material preparation and functionalisation of the MNs leading to complex fabrication methods. Therefore, MNs coupled with iontophoresis is an attractive combination as the iontophoresis allows an enhancement of the release by the migration of the drug and the MNs permit the physical disruption of the skin barrier (*i.e. stratum corneum*). Recently, porous MN patches have demonstrated a synergistic effect of the two technologies by improving insulin delivery.[11,31] Another porous MN patch was utilised for the delivery of dextran as well as the extraction of glucose by taking advantage of the transdermal electroosmotic flow generated by an iontophoresis patch.[34] Electroosmotic flow is an elegant and effective phenomenon generated when the pores in the MN are negatively charged. As the electroosmotic effect is higher than the electrophoretic mobility (charge migration)

upon an applied electric field, positively and negatively charged drugs can be delivered from the anode to the cathode. Following this approach, protein such as albumin (*i.e.* negatively charged) was successfully delivered.[35] Moreover, ovalbumin as a model vaccine was successfully injected by employing the electroosmotic flow-promoted intradermal delivery.[36] All these systems used porous MNs to electrically connect the drug-loaded reservoir with ISF and deliver macromolecules. Therefore, the enhanced delivery of small molecules is still unexplored with hollow MNs coupled with iontophoresis.

Herein, we report for the first time an iontophoretic hollow microneedle array system (IHMAS) for the on-demand delivery of charged drugs through the skin (Fig. 1A). Importantly, the working principle of the device is tested on positively and negatively charged drugs showing the versatility of the design to deliver different targets. Moreover, we prove the enhanced delivery of small molecules and proteins. Thus, the IHMAS system was tested for the delivery of model drugs such as methylene blue and lidocaine hydrochloride as positively charged molecules, and fluorescein sodium and BSA-FITC as negatively charged molecules. First, the on-demand delivery was characterised *in vitro* in an agarose gel (Fig. 1B), and later tested *ex vivo* for skin permeation by using porcine skin in a Franz diffusion cell setup (Fig. 1C). Finally, the miniaturization of the anode and cathode for the full integration of the iontophoretic system in a single IHMAS (Fig. 1D) was attained and
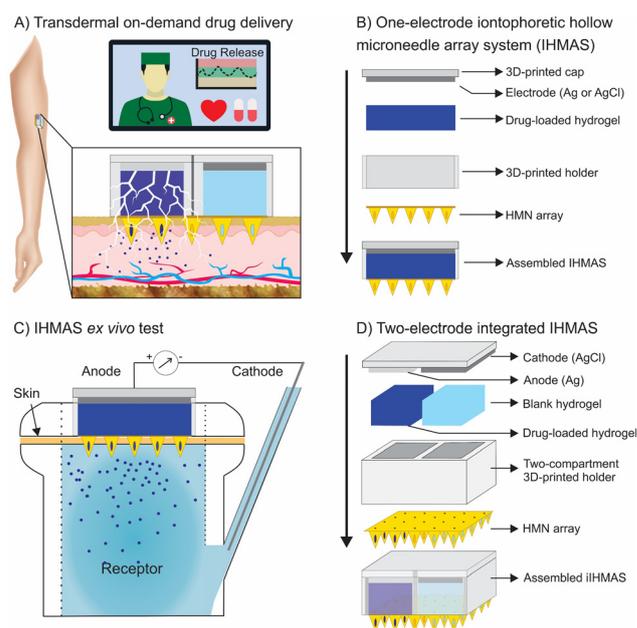

Fig. 1 Illustration of the iontophoretic hollow microneedle array system (IHMAS). (A) Concept of transdermal on-demand drug delivery for personalised therapy. (B) Design of the single electrode IHMAS employed to test the delivery principle. (C) Franz diffusion cell configuration used during the *ex vivo* test. (D) Schematic of the integrated IHMAS consisting of the anode and the cathode in the same HMN patch for on-demand drug delivery.

successfully tested *ex vivo* overall, the iontophoretic system has been integrated into a HMN array for successful on-demand delivery of drugs which will provide an advent in personalised therapy.

Experimental

Fabrication and characterisation of HMNs.

The HMN arrays were designed using Shapr3D. The arrays consist of 5 × 5 HMNs that have a pyramidal shape with 1 mm height, 0.75 mm width, 2 mm tip-to-tip interspacing, and 100 μm hole diameter (Fig. 2A). The HMN arrays were fabricated from polyether ether ketone (PEEK) sheets which were machined using a nanosecond-pulse, diode-pumped, solid-state laser operating at a wavelength of 355 nm (Fig.
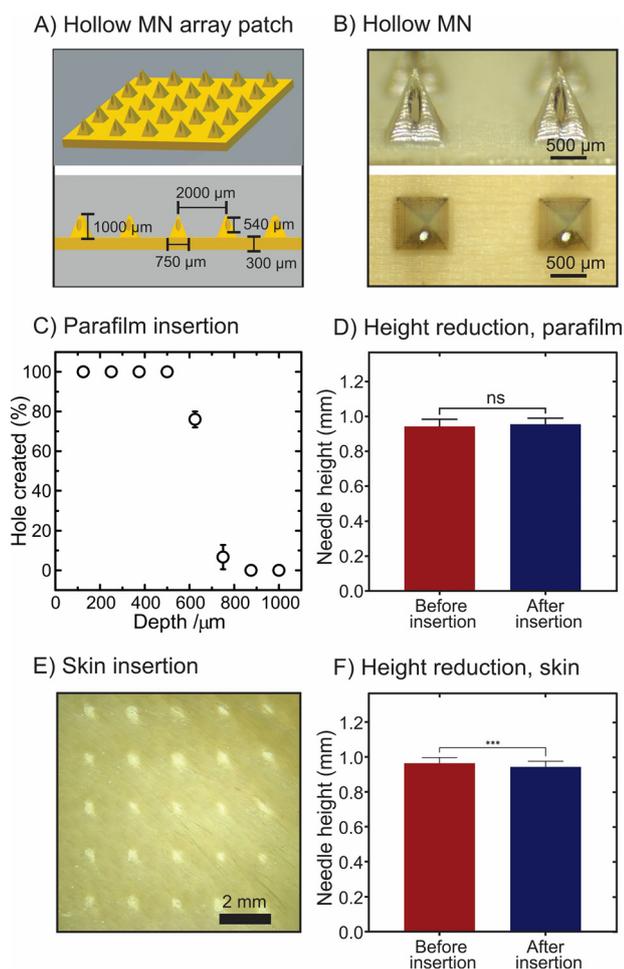

Fig. 2 Hollow microneedle (HMN) array patch and evaluation of the insertion capability. (A) Schematic of the HMN array (25 MNs) and its dimensions. (B) Representative images of the HMNs from the front view and top view. (C) Percentage of holes created by the HMN arrays observed in Parafilm M® insertion test. (D) Evaluation of the height reduction before and after the Parafilm M® insertion test (p-value > 0.05). (E) Image of the full-thickness porcine skin post-insertion test. (F) Evaluation of the height reduction before and after the skin insertion test (p-value < 0.05). ns: not significant. All data are presented as means ± standard deviations ($N = 3$).

S1†). The drilling of the holes was performed by the same laser system. The morphology and dimensions of the HMN arrays were assessed and measured using a digital light microscope (Leica EZ4 D, Leica Microsystems, Milton Keynes, UK). Moreover, a MN holder for fluid delivery was built to prove the HMN array allows fluids to pass through it (Fig. S2†). The information on the reagents, instrumentation, fabrication of the holder and methodology used for the mechanical testing are described in the ESI.†

Fabrication of the iontophoretic hollow microneedle array system

A 3D-printed holder was built to accommodate the HMN array (details of the fabrication and dimensions can be found in the ESI,† Fig. S3A and S3B). The function of the holder is to create a reservoir to load the target drug (Fig. S4A†). As the target drug needs to be in a solid-state electrolyte, the drug was loaded in an agarose hydrogel (details are described in the following sections). The drug-loaded hydrogel was subsequently added into the reservoir and capped with the proper electrode with an area of 1 cm^2 (Fig. 1B). The cap containing the electrode was made by 3D-printing (Fig. S4B†) and later painted with a suitable conductive paste (*i.e.* silver –Ag– for the anode and silver chloride –AgCl– for the cathode). Thereafter, the conductive paste was cured in the oven at 80 °C for 30 min. To test the concept, an entire IHMAS containing a single electrode was designed (Fig. 1C). Images of the assembly of the IHMAS are shown in Fig. S5.† After that, the integration of both anode and cathode in the same IHMAS was attained by dividing the HMN array into two sections to have two compartments (Fig. S3C and S3D for dimensions and S6A†), one for the anode electrode (36 mm^2) and another with the cathode electrode (36 mm^2) (Fig. 1D). This new holder was also produced by 3D-printing. In this case, the cap is also separated into two electrodes (Fig. S6B†) which were painted one with Ag and the other with the AgCl conductive pastes. In this way, the IHMAS is fully integrated into a single IHMAS device (Fig. S7†).

The iontophoretic principle in the microneedle array

Iontophoresis-based drug delivery consists of a two-electrode setup (*i.e.* anode and cathode) connected to a current source.[5] The electrochemistry used in this iontophoresis setup is widely studied using the Ag/AgCl couple.[6] In brief, electrodes used in this setup involve a Ag electrode as the anode and a AgCl electrode as the cathode. The electrochemical reaction occurring at the anode comprises the oxidation of the Ag(s) into Ag$^+$. Hence, when a positively charged drug is loaded at the anode, the drug is repulsed outwards the anode. In contrast, the electrochemical reaction occurring at the cathode consists of the reduction of the AgCl, thus Ag$^+$ into Ag(s), generating chloride ions which in turn repulse negatively charged drugs potentially loaded onto the cathode compartment outwards into the skin. In this work, methylene blue and lidocaine hydrochloride are used

as positively charged drugs and loaded on the anodal compartment. In contrast, fluorescein sodium and BSA-FITC as negatively charged molecules are loaded onto the cathodal compartment. It is worth mentioning that the concentration of the background electrolyte in the drug-loaded electrolyte was kept similar to physiological levels to avoid diffusion of the ions from the ISF to the IHMAS. However, a lower concentration of the electrolytes in the hydrogel might increase the efficiency of the drug delivery.

Traditional iontophoretic skin delivery systems can cause skin irritation, and mild to moderate skin erythema upon exposure to high and long iontophoretic currents directly on the skin.[5] The necessity of high and long currents to deliver proper amounts of drugs through the skin is due to the low permeability and hydrophobicity of the *stratum corneum*.[5] For this reason, piercing the *stratum corneum* of the skin with a MN array can create hydrophilic channels that facilitate a more effective drug delivery directly to ISF decreasing the time to deliver the desired dose.[3] Hence, the synergic combination of iontophoresis and MNs is studied in this work.

Preparation of the drug-loaded hydrogel

Drug-loaded agarose gel was prepared by dispersing 0.5 g agarose powder in 50 mL PBS solution (pH 7.4) at room temperature. The polymer solution was subsequently heated using a microwave for 2 min. Except for BSA-FITC, the drug powder was then dissolved in the agarose solution when the temperature of the solution was approximately 40 °C. The drug-agarose solution was cast onto a Petri dish and allowed to form a gel at room temperature. The percentage of drug loading is 0.5% w/v for all molecules. For BSA-FITC, a blank agarose gel was prepared following the same procedure. After the agarose gel formed, the 1% solution of BSA-FITC in PBS (pH 7.4) was added to the gel (1 : 1) and incubated overnight at room temperature to reach a 0.5% BSA-FITC loaded hydrogel.

In vitro drug delivery study

Agarose gel (1.5% w/v in PBS) was used as a model matrix for the *in vitro* tests. The agarose solution in PBS (pH 7.4) was microwaved until a clear solution was obtained. Subsequently, 50 mL of the solution was poured into a Petri dish. Once the hydrogel is solidified, the IHMAS can be pierced into the hydrogel to assess the delivery. The same device was used for the control and the iontophoresis condition. After the experiment, a skin puncher (8 mm diameter) was used to extract the agarose hydrogel where the drug was delivered (Fig. S8†). To quantify the amount delivered, the hydrogel sample was immersed in 1 mL PBS (pH 7.4) and let the drug diffuse for 24 h. Thereafter, the target drug in the control and the iontophoretic condition were quantified to assess the effect of the current on the IHMAS concept.

The quantification of methylene blue, fluorescein sodium and BSA-FITC was performed using a plate reader (FLUO star Omega, BMG LABTECH, UK). The concentration of

methylene blue was measured using an absorbance mode at 668 nm. The concentrations of fluorescein sodium and BSA-FITC were measured using a fluorescence mode with an excitation wavelength of 485 nm and an emission wavelength of 520 nm. The quantification of lidocaine hydrochloride was accomplished by using screen-printed electrodes (SPEs) fabricated in-house.[28] Briefly, a screen-printed machine (DEK NeoHorizon 01iX, Assembly Systems GmbH, Germany) was used to print working and counter electrodes with carbon ink and Ag/AgCl for the pseudoreference electrodes on a PET substrate.

Ex vivo drug permeation study

Franz diffusion cells are a well-established setup for drug delivery studies.[3] In this work, *ex vivo* permeation studies for methylene blue, fluorescein sodium, BSA-FITC, and lidocaine hydrochloride were carried out using Franz diffusion cell apparatus with dermatomed neonatal porcine skin (500 μm). Porcine skin was thawed in PBS (pH 7.4) and allowed to equilibrate at room temperature before attaching it onto the donor compartment using cyanoacrylate glue. The receptor compartment was filled with PBS (pH 7.4) and agitated at 600 rpm using a magnetic stirrer bar and equilibrated to 37 ± 1 °C. The IHMAS was then inserted into the neonatal porcine skin using manual force for 30 s. A 16 g metal weight was placed on the cap of the MN holder to ensure the IHMAS remained inserted throughout the experiment (*i.e.* 6 h). Subsequently, the donor compartment was carefully placed on top of the receptor compartment and a steel clamp was used to secure them without creating an air bubble below the skin. Parafilm® M was used to cover the opening of the donor compartment and the sampling arm of the receptor compartment to reduce water loss through evaporation. The samples (300 μL) were taken from the receptor compartment at predetermined time points and replaced with an equal volume of fresh PBS (pH 7.4) to maintain the volume of 20 mL. The samples were analysed using a plate reader or SPEs as appropriate. Fig. S9† displays all the elements in the Franz diffusion cell.

Drug extraction from the skin samples

The extraction of model drugs from the porcine skin was performed to quantify the amount of each drug that was deposited on the skin post-microneedle removal after 6 h. Briefly, the skin samples were removed from the donor compartment of the Franz diffusion cell and individually placed in a 2 mL Eppendorf tube. A 0.5 mL of deionised water and two pieces of stainless beads were placed in the tube containing the skin. The first homogenisation step was carried out with the help of Tissue Lyser LT (Qiagen Ltd., Manchester, UK) at 50 Hz for 15 min. Subsequently, 1 mL methanol was added to the above mixture and homogenised again using the Tissue Lyser LT at 50 Hz for 15 min.[37] The mixture of each sample was transferred to a 15 mL Falcon tube containing 8.5 mL of methanol. The tubes were then sonicated for 24 h at

room temperature to extract all of the model drugs from the skin. All the samples were vortexed for 30 s, and then 2 mL of the sample were taken to be centrifuged at 15 300 rpm for 15 min. Finally, the supernatant of the samples was collected and analysed using a plate reader or SPEs with the setups as previously described.

Statistical analysis

Statistical analysis was performed using GraphPad Prism version 9.4.0 (GraphPad Software Inc., San Diego, CA). This included calculations of the means and standard deviations, with an unpaired t-test with Welch's correction or a one-way analysis of variance (ANOVA), followed by a multiple comparison test (Tukey's test) to assess whether there were significant differences between the means of the data sets as appropriate. In all cases, $p < 0.05$ denotes statistical significance.

Results and discussion

Design and characterisation of the HMN array

The morphology and dimensions of the HMN array fabricated with PEEK was observed and measured using a digital light microscope (Fig. 2B). The array consists of 25 pyramidal HMNs with a height of 994 ± 56 μm and a hole diameter of 94 ± 7 μm. Table S1† shows the dimensions of the HMNs in computer-aided design (CAD) and when measured with the microscope. It was observed that the dimensions of the resulting HMN arrays showed small deviations from the CAD. The deviation of HMNs' dimensions as a result of the production method (*i.e.* laser micromachining) was previously reported.[28] The percentages of the deviations ($N = 3$) for the HMN arrays were 0.6% (needle height), 1.9% (needle width), 1.2% (tip-to-tip interspacing), 3.7% (baseplate thickness), 6.0% (hole diameter bottom), and 6.5% (hole diameter on MN body). Parafilm M® model[38] and full-thickness neonatal porcine skin model were used to assess the insertion ability of the HMNs.[39] Firstly, the HMNs could penetrate eight layers of Parafilm M® with an insertion depth of 625 μm (Fig. 2C). This implies that 62.9% of the needle height was inserted when the insertion force is 32 N array^{-1}. The morphology and the needle height did not significantly change after the insertion (943 ± 41 μm *versus* 955 ± 35 μm, p-value > 0.05, Fig. 2D). The obtained insertion depths are in line with previously described insertion profiles for MNs with needle lengths ranging between 800 and 1000 μm.[38,40] The insertion depths obtained for this type of HMNs are higher than the ones reported for similar pyramidal HMNs prepared using 3D printing.[41] This could be due to needle sharpness as the needle tips described in this article are sharper than the 3D-printed HMNs described in the literature.[41]

Subsequently, the ability of the HMNs was also assessed in full-thickness neonatal porcine skin (*ca.* 600 μm thickness) supported by eight layers of Parafilm M® using the Texture Analyser with the insertion force of 32 N. Fig. 2E illustrates 25 holes created by the HMNs, suggesting that all HMNs on the array could pierce the outer layer of the skin and reach the skin depth of 600 μm. For the skin insertion test, the needle height was measured before and after insertion. Although there was a significant difference in the heights between pre- and post-insertion (964 ± 32 μm *versus* 943 ± 32 μm, p-value < 0.05, Fig. 2F), the difference (in absolute values) of the needle heights measured before and after insertion were marginal (*i.e.* 3%). This value is consistent with previously reported MN compression after insertion.[42]

Effect of applied current on the delivery of drug

The electrical-stimuli delivery of drugs by using iontophoresis depends on the charge of the target drug. During the application of a current between two electrodes, an electrochemical reaction occurs at each of the electrodes leading to the migration of certain ions.[4] In this work, HMNs are used to pierce the skin and reach the dermis layer of the skin, thus depositing the drug directly to the ISF and enhancing the drug absorption process. As certain drug molecules are positively or negatively charged at physiological conditions (*i.e.* pH 7.4), the electrochemical reaction on the electrodes generates the migration of the drug towards the ISF. Thus, the migration of charged molecules is the principle that is used in the IHMAS to enhance the delivery of several drugs.

After proving the capability of the HMNs to pierce the skin, the HMN array was mounted on the 3D-printed holder to create the iontophoretic setup (Fig. S5†). A simple arrangement was first assessed by using the entire HMN array as a single electrode to prove the electrorepulsion principle. Depending on the model molecule that is delivered, a different electrode must be used. Therefore, a positively charged drug is loaded in the reservoir of the anode and a negatively charged drug in the cathode. Several drugs were tested to prove the versatility of the IHMAS. As positively charged molecules loaded at the anode, methylene blue and lidocaine hydrochloride were employed. As negatively charged molecules loaded at the cathode, fluorescein sodium was used. Moreover, to prove that the system can also enhance the delivery of macromolecules (*e.g.* proteins), BSA labelled with FITC for proper quantification was employed as the model, which at physiological pH it is negatively charged, and thus loaded at the cathode.

The principle was evaluated *in vitro* by using a 1.5% agarose gel. First, methylene blue was employed as it allows its simple quantification by spectroscopic methods (*i.e.* absorbance measurement). The drug-loaded gel was deposited on the HMN holder under an anode configuration (Ag electrode). In this case, a AgCl wire was used as a cathode. The effect of the current exhibited an increase in the delivery upon increasing the current showing the impact of the migration principle on the delivery of the positively charged drug (Fig. S8A†). The increase of the delivery was enhanced from 5-fold by applying 0.1 mA cm^{-2} up to 30-fold by applying 1 mA cm^{-2} (Fig. 3A). The range of current density from 0.1 to 1 mA cm^{-2} was selected because higher values have been reported to cause skin
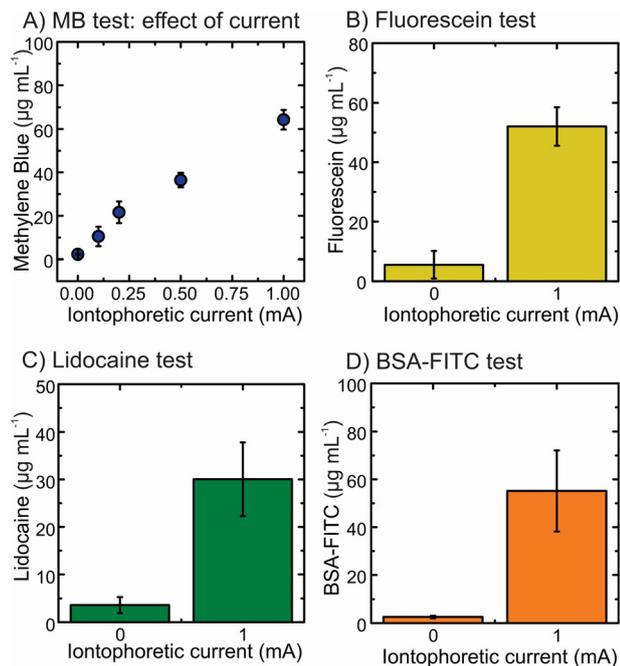
Fig. 3 *In vitro* test on agarose gel for electrically-induced drug delivery using the iontophoretic hollow microneedle array system (IHMAS). (A) Effect of the iontophoretic current on the delivery of methylene blue (MB) for 1 h. Enhanced delivery after the application of 1 mA for 1 h on the IHMAS loaded with (B) fluorescein sodium, (C) lidocaine hydrochloride, and (D) BSA-FITC. The area of the electrode is 1 cm^2. Data are presented as means ± standard deviations (N = 3).

irritation.[43] Moreover, the higher the current, the higher the power consumption which can limit the wearable configuration in future miniaturisation.[44] The current density of 1 mA cm^{-2} was chosen for further experiments as it provides the highest delivery of drug in comparison to the control experiment (0 mA cm^{-2}). Thereafter, the cathode configuration was tested with fluorescein sodium as a negatively charged model drug loaded in the reservoir and using a Ag wire as the anode (Fig. S8B†). This cathode configuration resulted in a 10-fold enhancement in the delivery of fluorescein sodium, as shown in Fig. 3B. Subsequently, lidocaine hydrochloride was used as a model of local anaesthetic. Lidocaine hydrochloride, as a positively charged drug at pH 7.4, was added to the anode compartment. A 10-fold increment on the delivery was obtained after applying 1 mA cm^{-2} (Fig. 3C). Finally, a negatively charged macromolecule (*i.e.* BSA-FITC) was used to show the capability of the system to deliver proteins (Fig. S8C†). In this case, a 20-fold increase in the delivery was attained showing that the iontophoresis also works with charged macromolecules (Fig. 3D). The increments in the delivery differ from molecule to molecule as each molecule has different hydrophilic properties thus it can diffuse easily through the hydrogel as well as it might depend on the size of the molecule and the charge of the molecule. Target drugs with higher water solubility and charge are favourable for iontophoretic delivery.[5] Therefore, the model drug delivery cannot be compared and need to be studied case by case.

Ex vivo drug permeation study

Porcine skin was used for the *ex vivo* test to emulate transdermal drug delivery through the skin as it is the most physiologically similar to human skin.[45] For this purpose, a Franz diffusion cell setup was used by introducing dermatomed porcine skin in between the donor and receptor compartments (Fig. S9†). In this test, the single electrode setup was employed to validate the principle in porcine skin. After incubating the skin in PBS for 15 min, the IHMAS device was inserted into the skin by the application of manual pressure for 30 s. In parallel, control devices (*i.e.* without current application) and devices with 1 mA cm^{-2} applied current were employed in the test for 6 h (Fig. S10†). First, methylene blue was used as the cationic model drug in the anode compartment in the Franz diffusion cell (Fig. 4A). To prove a similar behaviour to the *in vitro* test, an evaluation of the effect of applied current to the system was executed. Fig. 4B depicts the concentration of methylene blue found in the receptor compartment of the Franz diffusion cell at each time point on four conditions of applied current (*i.e.* 0 mA, 0.1 mA, 0.5 mA and 1 mA) using the 1 cm^2 electrode. During the application of current at 1 mA, the concentration of methylene blue reached a plateau after 5 h (31.1 ± 6.3 μg mL^{-1}). This is aligned with less permeation of methylene blue during the application of 0.5 mA current, which constantly delivered the drug during the 6 h without reaching a plateau (6 h, 25.8 ± 3.5 μg mL^{-1}). The plateau suggests that the rate of the electrochemical reactions occurring at the Ag and AgCl electrodes decreased or stopped. After the experiments, the unmounted system unravelled that the Ag electrode was almost completely oxidized as its colour transitioned from light grey (Ag) to dark grey (AgCl). However, this effect needs to be further evaluated to understand whether the target drug influences the electrochemical reaction rate. Furthermore, the condition at 0.1 mA did not significantly improve the permeation of methylene blue in comparison to the control experiment as a small current was applied (6 h, 2.4 ± 0.3 μg mL^{-1} *versus* 0.5 ± 0.1 μg mL^{-1}, N = 3, p-value > 0.05). After 6 h of the current application, the 0.1 mA, 0.5 mA and 1 mA conditions could increase the delivery of methylene blue up to 4 times, 49 times and 61 times when compared to the control experiment, respectively. However, the effect of applied current on drug permeation was significantly notified only when 0.5 and 1 mA currents were used (p-value < 0.05). The results from the *ex vivo* study were similar to those found in the *in vitro* test (Fig. 3A). Consequently, the current of 1 mA cm^{-2} was selected in all subsequent experiments.

Fluorescein sodium, as a negatively charged drug, was loaded in the cathode IHMAS device to evaluate the enhanced permeation in the *ex vivo* setup by applying 1 mA cm^{-2} current (Fig. S11†). This device exhibited a constant and linear delivery of the drug during the 6 h of the current application (Fig. 4C). A 43-fold significant increase in the permeation of fluorescein sodium was obtained after 6 h of the current application in comparison to the control (66.1 ± 12.0 μg mL^{-1} *versus* 1.5 ± 0.5
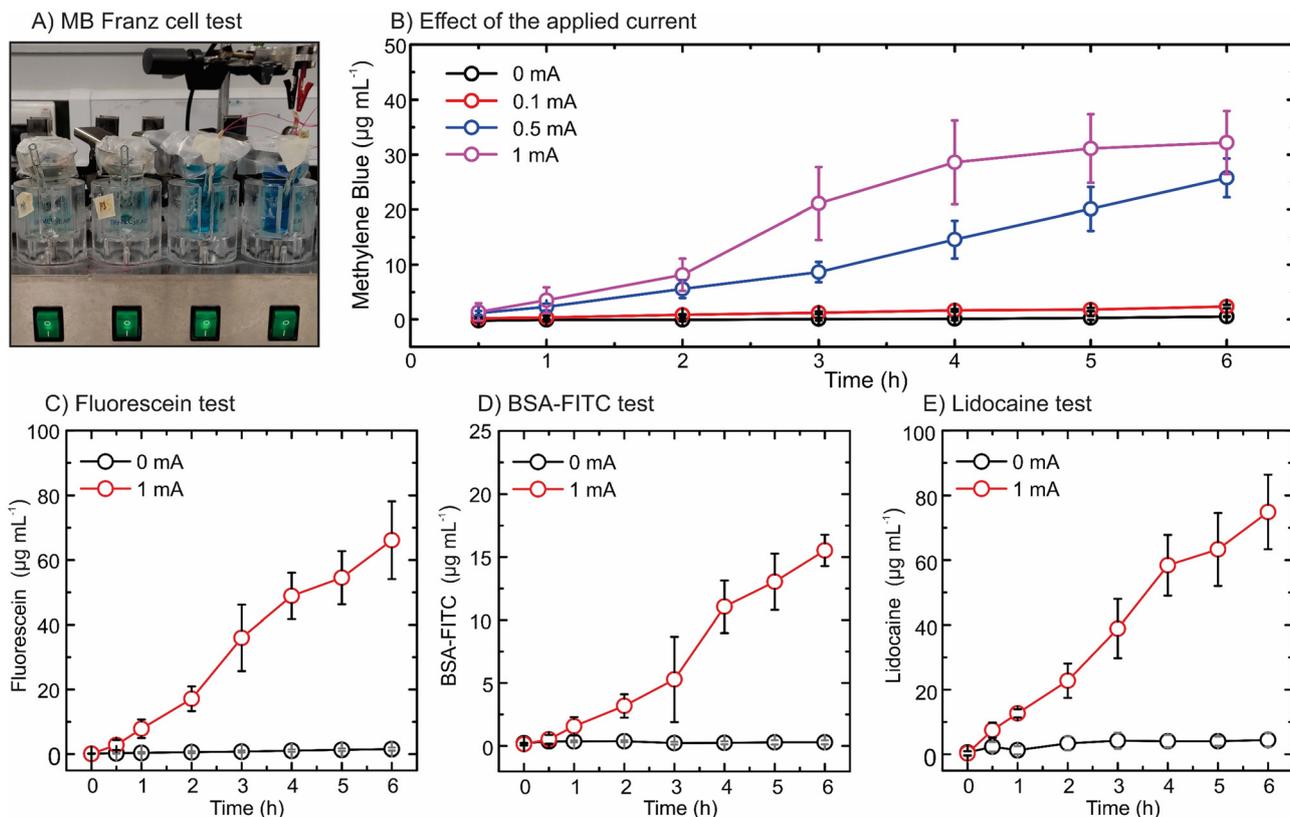
Fig. 4 *Ex vivo* permeation test using Franz diffusion cells. (A) Image of the Franz diffusion cell setup. (B) Effect of the applied current on the permeation of methylene blue through the skin (means ± standard deviations, $N = 3$). Enhanced permeation of (C) fluorescein sodium, (D) BSA-FTIC, and (E) lidocaine hydrochloride while applying 1 mA of iontophoretic current on the hollow microneedle iontophoretic patch during 6 h. Data are presented as means ± standard deviations, $N = 4$.

$\mu g \ mL^{-1}$, $N = 4$, p-value < 0.05). Thereafter, the IHMAS in cathode configuration was loaded with BSA-FITC to assess the effect of the applied current on the skin permeation of the macromolecule (Fig. S12†). Fig. 4D depicts the permeation profile of BSA-FITC, which significantly increased after 6 h current application compared to the control ($15.5 \pm 1.3 \ \mu g \ mL^{-1}$ *versus* $0.3 \pm 0.2 \ \mu g \ mL^{-1}$, $N = 4$, p-value < 0.05). This demonstrates that the iontophoresis system could enhance transdermal delivery of BSA-FITC by 54 fold. It was also observed that the concentration of BSA-FITC found in the receptor compartment was significantly less than those of fluorescein sodium and methylene blue (p-value < 0.05). This is potentially related to the size of the macromolecule that hinders the migration of BSA-FITC through the skin.

Finally, lidocaine hydrochloride was tested in the anode compartment as a positively charged molecule. Permeation profiles upon application of the current and the control during 6 h are shown in Fig. 4E. After exhibiting a constant increase in the delivery through time, a 17-fold significant increment in the permeation of lidocaine hydrochloride was obtained at a 6 h time point ($74.8 \pm 11.5 \ \mu g \ mL^{-1}$ *versus* $4.4 \pm 2.2 \ \mu g \ mL^{-1}$, $N = 4$, p-value < 0.05).

In this study, the control experiments of lidocaine hydrochloride showed higher skin permeation after 6 h than methylene blue and BSA-FITC ($4.4 \pm 2.2 \ \mu g \ mL^{-1}$ *versus* $0.5 \pm$

$0.1 \ \mu g \ mL^{-1}$ and $0.3 \pm 0.2 \ \mu g \ mL^{-1}$, respectively, p-value < 0.05). These results might be due to several factors. First of all, lidocaine hydrochloride is relatively hydrophilic (*i.e.* $\log P = 2.84$) in its cationic form. Therefore, it can easily diffuse through the skin to the receptor compartment more than methylene blue which is relatively more hydrophilic ($\log P = -0.62$). For BSA-FITC, less skin permeation is a result of larger molecular size when compared to lidocaine hydrochloride (66 kDa *versus* 288.81 Da). Similar findings were observed in the samples treated with 1 mA cm^{-2} current. Thus, the differences in drug properties including hydrophilicity and molecular size affect skin permeation regardless of the application. The iontophoretic approach used in this work has been proven to dramatically enhance the permeation of different types of molecules, demonstrating the versatility of the IHMAS.

The total amount of drugs delivered by the IHMAS

The IHMAS device enhanced the skin permeation of the drugs *via* two mechanisms: (i) HMNs bypassed the *stratum corneum* and reached the dermis layer, and (ii) the drug loaded in the hydrogel reservoir was delivered by the repulsive force generated at the electrode when the current was applied. Ideally, the drug travels from the reservoir to the dermis, in

which ISF and microcirculation are located. In the case of the *ex vivo* experiment, the amount of drug permeated across the skin was typically quantified from the PBS situated in the receptor compartment of the Franz diffusion cell. However, some drugs might be deposited in the skin as this physical barrier might entrap some of the electrical stimuli delivered drug. According to the hydrophilicity and size of molecules, drugs can be retained in the skin at different magnitudes. Therefore, it is important to quantify not only the amount of drug in the receptor compartment of the Franz diffusion cell but also the amount of drug retained in the skin to obtain the total amount of drug delivered with the IHMAS.

To untangle the total amount of drug delivered by the IHMAS device, the drug retained in the porcine skin during the *ex vivo* experiment was extracted and quantified for both the control and the applied current samples. The total amount of each molecule delivered through the IHMAS in the receptor compartment and retained in the porcine skin is displayed in Fig. 5. A summary containing the total amount of drug delivered (considering the skin and the receptor compartment) which was employed to calculate the delivery yield of the IHMAS is shown in Table 1.

Concerning the tests employing small molecules, methylene blue, which is the most hydrophilic compound used in this work (log P = −0.62), was delivered in the least quantity in the iontophoretic condition (728.6 ± 108.6 μg methylene blue *versus* 1384.6 ± 269.3 μg fluorescein sodium and 1513.7 ± 234.8 μg lidocaine hydrochloride, *p*-value < 0.05). As previously reported, the diffusion of dyes such as methylene blue through the skin is hindered by the interaction of methylene blue ions with proteins from the tissue.[46] Indeed, methylene blue is more likely to be retained in the skin due to the lipophilic nature of the skin.[47,48] The delivery of methylene blue using MN arrays

has been described previously using hydrogel-forming MN arrays and dissolving MN arrays.[49,50] The methylene blue-loaded dissolving MN arrays (196 individual MNs per array) rapidly delivered approximately 3.6 mg of methylene blue upon the dissolution of polymers after 30 min application. It was observed that dissolving MN arrays delivered a greater amount of methylene blue to porcine skin in a shorter period compared to the IHMAS described herein due to higher MNs per array, greater drug loading, and more skin contact area. Additionally, the nature of dissolving MNs is that the polymer dissolves in the skin and releases drug encapsulated, while no element of the IHMAS dissolved. In general, dissolving MN arrays are designed for the rapid delivery of the active substance. To use dissolving MN arrays as a controlled drug delivery system, polymers with slow dissolution profiles or drug nanocarriers are required.[51] Another study showed that the iontophoresis system could also enhance the skin permeation of methylene blue when used in combination with hydrogel-forming MN arrays.[50] When 0.5 mA current was applied, the hydrogel-forming MN arrays (9 MNs per array) facilitated the skin permeation of methylene blue loaded in the adhesive layer (3 mg cm^{-2}) to reach approximately 1000 μg in 6 h. The different magnitude of enhancement in skin permeation between the hydrogel-forming MN system and our IHMAS could be due to dissimilarity in drug release mechanism. The hydrogel-forming MNs directly contacted the skin and allowed omnidirectional drug diffusion to take place. In contrast, the drug in HMNs travels through microsized channels driven by the repulsion force and reaches the skin layers in one direction. Although there are differences in the mechanism and surface area for drug delivery between hydrogel-forming MN arrays and HMN arrays, both systems proved the enhanced delivery of methylene blue using an iontophoretic system. As demonstrated in methylene blue, different delivery methods based on MNs allow different delivery profiles. Dissolving MNs exhibit a rapid delivery for short time administration by dissolving the polymer and the drug directly in the skin, hydrogel-forming MNs need time to get hydrated, but once hydrated by interstitial fluid, they can deliver a high amount due to omnidirectional diffusion or migration (in case of the coupling with iontophoresis) from the reservoir to the skin, and hollow MNs acts as a carrier for easy penetration of the skin with immediate availability for drug delivery from the reservoir by diffusion and/or migration.

Interestingly, fluorescein sodium and lidocaine hydrochloride were delivered at the highest total amount with the iontophoretic system described in this study (1384.6 ± 269.3 μg and 1513.7 ± 234.8 μg for fluorescein sodium and lidocaine hydrochloride, respectively). The permeation of both molecules across the porcine skin to the receptor compartment of Franz diffusion cells was relatively comparable (1322.2 ± 240.9 μg for fluorescein sodium and 1496.9 ± 229.9 μg for lidocaine hydrochloride, N = 4, *p*-value > 0.05). Moreover, the amounts of these molecules in the skin after 6 h current application were considered similar (62.4 ± 42.5 μg for fluorescein sodium and 16.8 ± 6.0 μg for
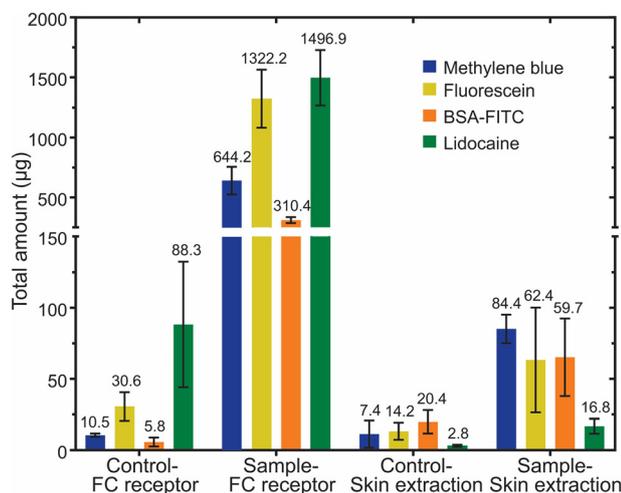

Fig. 5 Total amount of drug delivered by the IHMAS device. The amount of drug was quantified from the samples obtained from the receptor compartment of Franz diffusion cell (FC) and the drug extraction from the porcine skin after 6 h of the iontophoretic transdermal delivery. Data are presented as means ± standard deviations, N = 4 (N = 3 for methylene blue). The numbers shown above each bar graph indicate mean values.

Table 1 The total amount of drug delivered and delivery yield using the IHMAS device. Data of the total amount of drug delivered are presented as means ± standard deviations (SD); $N = 4$ except $N = 3$ for methylene blue. The delivery yield is calculated from the total amount of drug loaded in the hydrogel (*i.e.* 1620 μg per reservoir)

Model drug	The total amount of drugs delivered (mean ± SD, μg)		Delivery yield (%)	
	Control	Iontophoresis	Control	Iontophoresis
Methylene blue	18.0 ± 6.5	728.6 ± 108.6	1.1	45.0
Fluorescein sodium	44.8 ± 4.7	1384.6 ± 269.3	2.8	85.5
Lidocaine hydrochloride	91.1 ± 44.3	1513.7 ± 234.8	5.6	93.4
BSA-FITC	26.1 ± 9.9	370.1 ± 31.2	1.6	22.8

lidocaine hydrochloride, $N = 4$, *p*-value > 0.05). The similarity in the delivery profiles of these molecules perhaps involves their molecular sizes and hydrophobicity that are in the same range (376.27 Da and $\log P$ 2.65 for fluorescein sodium, and 288.81 Da and $\log P$ 2.84 for lidocaine hydrochloride). A small amount of lidocaine hydrochloride was encountered in the skin, indicating its fast diffusion through the skin. These results are comparable with the results reported by Garland *et al.* for dissolving MN arrays after 6 h.[52]

Finally, the total amount of BSA-FITC delivered by using the IHMAS was significantly increased when compared to the control ($N = 4$, *p*-value < 0.05). The results show that the IHMAS delivered 370.1 ± 31.2 μg of BSA-FITC (59.7 ± 28.2 μg in the skin and 310.4 ± 25.0 μg in the receptor compartment) within 6 h. Whilst, the control could deliver only 26.1 ± 9.9 μg of BSA-FITC in the same duration (20.4 ± 9.4 μg in the skin and 5.8 ± 3.1 μg in the receptor compartment). The total amount of the protein delivered by the IHMAS was relatively lower than those of the small molecules. This potentially relates to the bigger size of the molecule, which hinders the transfer rate of the protein through the whole iontophoretic setup and hence the permeation through the skin. However, unexpectedly, the retention of BSA-FITC in the skin was comparable to the other drugs reported in this work when the iontophoretic system was used (*p*-value > 0.05). It was assumed that the larger size of the albumin would hinder the migration of the protein to the skin. However, it is suggested that the power of the iontophoretic system strongly assists in the permeation of the albumin from the IHMAS to the receptor compartment. Moreover, studies showed that albumin has higher adsorption with hydrophilic surfaces rather than hydrophobic surfaces[53] which could explain the low retention of the protein in the skin (*i.e.* lipophilic environment).[47] A previous study reported BSA-FITC delivery using hydrogel-forming MN arrays. The iontophoresis system with hydrogel-forming MN arrays could dramatically improve the skin permeation of a macromolecule such as BSA-FITC similar to our work when compared to the transdermal patch.[50] Moreover, Lee *et al.* described the use of dissolving MN arrays for the delivery of BSA-FITC, achieving results in line with the ones reported here.[54]

Although the direct comparison between the IHMAS device and other types of MN arrays cannot be conducted due to the differences in drug loading, type of MNs, surface

area, and mechanism of drug delivery, the results presented here suggest that the IHMAS can be used to activate an enhanced delivery of model molecules when compared to the HMN alone. Essentially, the novelty of this work relies on the versatility of the system to deliver different types of drugs, the ability to provide on-demand drug delivery, and importantly, the miniaturisation and integration of the electrodes in a single MN patch.

The delivery yield considers the volume of the drug-loaded hydrogel (0.324 mL of hydrogel fitting the dimension of the reservoir – 0.9 cm × 0.9 cm × 0.4 cm) and its concentration (5 mg mL^{-1}) to calculate the total amount of drug in the reservoir (*i.e.* 1620 μg). According to the total amount of drug delivered after 6 h of the iontophoretic activation, the delivery yield was 45.0% for methylene blue, 85.5% for fluorescein sodium, 93.4% for lidocaine hydrochloride, and 22.8% for BSA-FITC. As expected, the highest yields were attributed to small molecules as they can easily migrate from the reservoir to the receptor compartment. In contrast, proteins like BSA-FITC exhibited the lowest yield due to the size of the macromolecule.

Full integration of the two-electrode iontophoretic system in a IHMAS device

The coupling of the iontophoretic effect on HMN has been shown to provide a strong effect on the permeation of charged drugs through the skin. However, the work described in previous sections used a IHMAS device encompassing only one single electrode, either anode or cathode, in a single HMN patch and using a wire as the counter electrode. Hence, the integration of both electrodes in the same IHMAS is necessary for a fully deployable device in real scenarios. To tackle this challenge, a new MN holder was designed to embed both electrodes in the same HMN array (Fig. S7†). In this new configuration, the MN holder is divided into two reservoirs, having a septum in the middle of the HMN array (25 HMNs). The miniaturisation only allows for 10 HMNs at each electrode as the septum covers a column of 5 HMNs. Moreover, the height of the MN holder increased from 4.5 mm to 6.5 mm as well as the depth of the cap to increase the isolation of the hydrogels. This is a key layout to avoid mixing hydrogel/solution during iontophoresis as the connection of the cell by electrolyte solution would disrupt

the migration effect through the HMNs into the skin. The new design decreases the size of the electrode to 0.36 cm^2, thus having less area and volume for the electrode and drug-loaded hydrogel, respectively. The images of the HMN array arranged on the new two-electrode MN holder are shown in Fig. S7.†

Once the fully integrated IHMAS (iIHMAS) is devised (Fig. 6A), the iIHMAS device was preliminary tested *in vitro* by piercing it in the 1.5% agarose gel. Fig. 6B depicts the results of the control experiment (iIHMAS without current) and the applied current (1 mA cm^{-2}) ($N = 3$) for the delivery of a positively charged model drug (*i.e.* methylene blue). In this setup, methylene blue-loaded hydrogel is deposited on the anode compartment, and a blank hydrogel is deposited on the cathode compartment to close the cell. Interestingly, a 26-fold increment in the delivery of methylene blue was attained by the iontophoretic condition in comparison to the control indicating the suitability of the miniaturised design. Therefore, the proof of concept of all electrodes in one iIHMAS was successfully developed. Subsequently, the device was tested in an *ex vivo* setup to assess the skin permeation of the drug. Fig. 6C displays the schematics of the Franz diffusion cell setup with the iIHMAS piercing the skin. Upon the application of 1 mA cm^{-2} current to the cell, methylene blue started diffusing to the receptor compartment due to

the repulsion generated by the Ag$^+$ from the oxidation of the Ag(s) at the anode. The permeation of methylene blue through the porcine skin was monitored for 6 h as it is shown in Fig. 6D. The enhanced permeation effect was significantly observed from 2 h iontophoresis ($N = 3$, p-value < 0.05) and rapidly increased until 4 h, which later started a decrease in the delivery rate until 6 h. In comparison with the control condition that exhibited a steady low delivery of methylene blue, the iIHMAS attained 18 times more skin permeation at 6 h (0.5 ± 0.2 µg mL^{-1} *versus* 9.3 ± 0.4 µg mL^{-1}, $N = 3$, p-value < 0.05). Another test was performed by using a negatively charged drug molecule (*i.e.* fluorescein sodium). In this case, the fluorescein sodium-loaded hydrogel was deposited in the cathode compartment and a blank hydrogel in the anode compartment. Fig. S13† depicts the increase in the fluorescein sodium permeation in comparison to the control experiment during 4 h showing that the new design also performs using cationic or anionic species. Therefore, the iIHMAS also demonstrated its performance in the *ex vivo* setup, showing promise for its use in future *in vivo* scenarios.

Conclusions

The synergy between iontophoresis and HMNs in a single device has been presented. The IHMAS empowers the delivery of different types of drugs (*i.e.* small molecules and macromolecules), showing a dramatic enhancement in comparison to the control experiment without iontophoresis. The advantages of the iIHMAS rely on: (i) the simple setup employing unmodified HMNs; (ii) the versatility of the system which only needs the drug-loaded hydrogel for the delivery of the specific drug; (iii) the use of highly robust polymeric HMNs made of PEEK; and last but not least (iv) the use of the Ag and Ag/Cl conductive inks to print the electrodes on the reservoirs as a cost-effective material for scalable purposes. First, the evaluation of the IHMAS in agarose gel showed the enhanced effect of applied current on drug delivery. Thereafter, the IHMAS was tested in porcine skin using an *ex vivo* configuration to assess the permeation behaviour of model drugs (*i.e.* methylene blue, fluorescein sodium, lidocaine hydrochloride and BSA-FITC). The results exhibited a 61-fold, 43-fold, 54-fold, and 17-fold significant increment in skin permeation 6 h post-current application for methylene blue, fluorescein sodium, lidocaine hydrochloride and BSA-FITC in comparison to control experiments, respectively. Moreover, the quantification of the total amount of drug delivered showed delivery yields of 45.0% for methylene blue, 85.5% for fluorescein sodium, 93.4% for lidocaine hydrochloride, and 22.8% for BSA-FITC from the drug-loaded hydrogels. The different delivery profiles and delivery yields depend on the nature of the model molecules, leading to lower yields when employing higher hydrophilic molecules and macromolecules.

While conventional transdermal iontophoretic systems exhibit limitations such as skin irritation and the restriction of the delivery of certain drugs (*e.g.* <12 kDa), MN-based
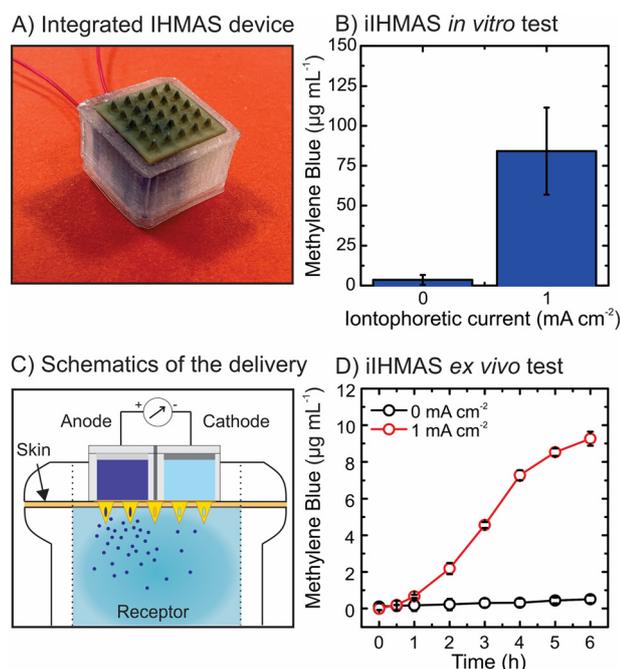

Fig. 6 Proof of concept of the two-electrode integrated iontophoretic hollow microneedle array system (iIHMAS). (A) Image of the iIHMAS device with two electrodes and the two-reservoir setup. (B) *In vitro* test of the iIHMAS device employing methylene blue for drug delivery. (C) Schematics of the *ex vivo* test for the iIHMAS device on a Franz diffusion cell. The drug-loaded hydrogel is situated in the anode compartment and a blank hydrogel is in the cathode compartment. (D) Skin permeation of methylene blue was observed over 6 h use of the iIHMAS device in a Franz cell setup. Data are presented as means ± standard deviations, $N = 3$.

iontophoretic systems can overcome these challenges by piercing the skin. On the other hand, these novel devices have still to address engineering endeavours such as manufacturing complexity, scalability and cost, or electrode lifespan. Overall, HMNs coupled with an iontophoretic system endows this IHMAS as a highly promising approach for transdermal on-demand drug delivery with the potential to improve patients' therapies and boost personalised healthcare.

Author contributions

Usanee Detamornrat, Marc Parrilla and Juan Domínguez-Robles: designing and performing experiments, methodology, analytical characterization, integration of the HMN array and iontophoresis system, and writing the manuscript. Qonita Kurnia Anjani: performing drug extraction from the skin and writing the manuscript: Eneko Larrañeta: writing the manuscript and supervision: Karolien De Wael and Ryan F. Donnelly: revision of the manuscript and supervision. The manuscript was written through the contributions of all authors. All authors have approved the final version of the manuscript.

Conflicts of interest

"There are no conflicts to declare".

Notes and references

1 M. R. Prausnitz and R. Langer, *Nat. Biotechnol.*, 2008, **26**, 1261–1268.

2 F. Sabbagh and B. S. Kim, *J. Controlled Release*, 2022, **341**, 132–146.

3 Y. Wang, L. Zeng, W. Song and J. Liu, *Drug Delivery Transl. Res.*, 2022, **12**, 15–26.

4 R. H. Guy, Y. N. Kalia, M. B. Delgado-Charro, V. Merino, A. López and D. Marro, *J. Controlled Release*, 2000, **64**, 129–132.

5 P. Bakshi, D. Vora, K. Hemmady and A. K. Banga, *Int. J. Pharm.*, 2020, **586**, 119584.

6 Y. N. Kalia, A. Naik, J. Garrison and R. H. Guy, *Adv. Drug Delivery Rev.*, 2004, **56**, 619–658.

7 D. Ramadon, M. T. C. McCrudden, A. J. Courtenay and R. F. Donnelly, *Drug Delivery Transl. Res.*, 2022, **12**, 758–791.

8 A. M. Helmy, *J. Drug Delivery Sci. Technol.*, 2021, **61**, 102332.

9 A. R. Hegde, P. V. Rewatkar, J. Manikkath, K. Tupally, H. S. Parekh and S. Mutalik, *Eur. J. Pharm. Sci.*, 2017, **102**, 237–249.

10 K. C. Liu, C. R. Green, R. G. Alany and I. D. Rupenthal, *Int. J. Pharm.*, 2013, **441**, 687–692.

11 Y. Li, J. Yang, Y. Zheng, R. Ye, B. Liu, Y. Huang, W. Zhou and L. Jiang, *Acta Biomater.*, 2021, **121**, 349–358.

12 M. Bok, Z. J. Zhao, S. Jeon, J. H. Jeong and E. Lim, *Sci. Rep.*, 2020, **10**, 2027.

13 E. Larrañeta, R. E. M. Lutton, A. D. Woolfson and R. F. Donnelly, *Mater. Sci. Eng., R*, 2016, **104**, 1–32.

14 R. F. Donnelly, T. R. Raj Singh and A. D. Woolfson, *Drug Delivery*, 2010, **17**, 187–207.

15 Q. K. Anjani, A. D. Permana, Á. Cárcamo-Martínez, J. Domínguez-Robles, I. A. Tekko, E. Larrañeta, L. K. Vora, D. Ramadon and R. F. Donnelly, *Eur. J. Pharm. Biopharm.*, 2021, **158**, 294–312.

16 Q. K. Anjani, A. H. Bin Sabri, J. Domínguez-Robles, N. Moreno-Castellanos, E. Utomo, L. A. H. Wardoyo, E. Larrañeta and R. F. Donnelly, *Biomater. Adv.*, 2022, **140**, 213073.

17 K. Ita, *J. Drug Delivery Sci. Technol.*, 2018, **44**, 314–322.

18 Á. Cárcamo-Martínez, B. Mallon, J. Domínguez-Robles, L. K. Vora, Q. K. Anjani and R. F. Donnelly, *Int. J. Pharm.*, 2021, **599**, 120455.

19 Y. Chen, B. Z. Chen, Q. L. Wang, X. Jin and X. D. Guo, *J. Controlled Release*, 2017, **265**, 14–21.

20 P. Liu, H. Du, Y. Chen, H. Wang, J. Mao, L. Zhang, J. Tao and J. Zhu, *J. Mater. Chem. B*, 2020, **8**, 2032–2039.

21 V. Ebrahiminejad, P. D. Prewett, G. J. Davies and Z. Faraji Rad, *Adv. Mater. Interfaces*, 2022, **9**, 2101856.

22 G.-S. Liu, Y. Kong, Y. Wang, Y. Luo, X. Fan, X. Xie, B.-R. Yang and M. X. Wu, *Biomaterials*, 2020, **232**, 119740.

23 H. Teymourian, F. Tehrani, K. Mahato and J. Wang, *Adv. Healthcare Mater.*, 2021, **10**, 2002255.

24 F. Tehrani, H. Teymourian, B. Wuerstle, J. Kavner, R. Patel, A. Furmidge, R. Aghavali, H. Hosseini-Toudeshki, C. Brown, F. Zhang, K. Mahato, Z. Li, A. Barfidokht, L. Yin, P. Warren, N. Huang, Z. Patel, P. P. Mercier and J. Wang, *Nat. Biomed. Eng.*, 2022, **6**, 1214–1224.

25 M. Parrilla, M. Cuartero, S. Padrell, M. Rajabi, N. Roxhed, F. Niklaus and G. A. Crespo, *Anal. Chem.*, 2019, **91**, 1578–1586.

26 K. Y. Goud, C. Moonla, R. K. Mishra, C. Yu, R. Narayan, I. Litvan and J. Wang, *ACS Sens.*, 2019, **4**, 2196–2204.

27 M. Parrilla, A. Vanhooydonck, M. Johns, R. Watts and K. De Wael, *Sens. Actuators, B*, 2023, **378**, 133159.

28 M. Parrilla, U. Detamornrat, J. Domínguez-Robles, R. F. Donnelly and K. De Wael, *Talanta*, 2022, **249**, 123695.

29 P. Makvandi, R. Jamaledin, G. Chen, Z. Baghbantaraghdari, E. N. Zare, C. Di Natale, V. Onesto, R. Vecchione, J. Lee, F. R. Tay, P. Netti, V. Mattoli, A. Jaklenec, Z. Gu and R. Langer, *Mater. Today*, 2021, **47**, 206–222.

30 Xu Lingling, Y. Yang, Y. Mao and Z. Li, *Adv. Mater. Technol.*, 2022, **7**, 2100055.

31 J. Yang, Y. Li, R. Ye, Y. Zheng, X. Li, Y. Chen, X. Xie and L. Jiang, *Microsyst. Nanoeng.*, 2020, **6**, 112.

32 Q. Ouyang, X. Feng, S. Kuang, N. Panwar, P. Song, C. Yang, G. Yang, X. Hemu, G. Zhang, H. S. Yoon, J. P. Tam, B. Liedberg, G. Zhu, K. T. Yong and Z. L. Wang, *Nano Energy*, 2019, **62**, 610–619.

33 Y. Yang, L. Xu, D. Jiang, B. Z. Chen, R. Luo, Z. Liu, X. Qu, C. Wang, Y. Shan, Y. Cui, H. Zheng, Z. Wang, Z. L. Wang, X. D. Guo and Z. Li, *Adv. Funct. Mater.*, 2021, **31**(36), 2104092.

34 S. Kusama, K. Sato, Y. Matsui, N. Kimura, H. Abe, S. Yoshida and M. Nishizawa, *Nat. Commun.*, 2021, **12**, 658.

35 H. Abe, K. Sato, N. Kimura, S. Kusama, D. Inoue, K. Yamasaki and M. Nishizawa, *Adv. NanoBiomed Res.*, 2022, **2**, 2100066.

36 H. Terui, N. Kimura, R. Segawa, S. Kusama, H. Abe, D. Terutsuki, K. Yamasaki and M. Nishizawa, *J. Drug Delivery Sci. Technol.*, 2022, **75**, 103711.

37 Q. K. Anjani, A. H. Bin Sabri, N. Moreno-Castellanos, E. Utomo, Á. Cárcamo-Martínez, J. Domínguez-Robles, L. A. H. Wardoyo and R. F. Donnelly, *Biomater. Sci.*, 2022, **10**, 5838–5855.

38 E. Larrañeta, J. Moore, E. M. Vicente-Pérez, P. González-Vázquez, R. Lutton, A. D. Woolfson and R. F. Donnelly, *Int. J. Pharm.*, 2014, **472**, 65–73.

39 I. A. Tekko, G. Chen, J. Domínguez-Robles, R. R. S. Thakur, I. M. N. Hamdan, L. Vora, E. Larrañeta, J. C. McElnay, H. O. McCarthy, M. Rooney and R. F. Donnelly, *Int. J. Pharm.*, 2020, **586**, 119580.

40 S. N. Economidou, C. P. P. Pere, A. Reid, M. J. Uddin, J. F. C. Windmill, D. A. Lamprou and D. Douroumis, *Mater. Sci. Eng., C*, 2019, **102**, 743–755.

41 E. Mathew, G. Pitzanti, A. L. Gomes Dos Santos and D. A. Lamprou, *Pharmaceutics*, 2021, **13**, 1–14.

42 R. E. M. Lutton, E. Larrañeta, M. C. Kearney, P. Boyd, A. D. Woolfson and R. F. Donnelly, *Int. J. Pharm.*, 2015, **494**, 417–429.

43 T. K. Giri, S. Chakrabarty and B. Ghosh, *J. Controlled Release*, 2017, **246**, 30–38.

44 M. Parrilla and K. De Wael, *Adv. Funct. Mater.*, 2021, **31**, 2107042.

45 S. A. Ranamukhaarachchi, S. Lehnert, S. L. Ranamukhaarachchi, L. Sprenger, T. Schneider, I. Mansoor, K. Rai, U. O. Häfeli and B. Stoeber, *Sci. Rep.*, 2016, **6**, 1–9.

46 E. A. Genina, A. N. Bashkatov and V. V. Tuchin, in *ALT'03 International Conference on Advanced Laser Technologies: Biomedical Optics*, ed. R. K. Wang, J. C. Hebden, A. V. Priezzhev and V. V. Tuchin, 2004, vol. 5486, pp. 315–323.

47 G. B. Kasting, M. A. Miller, T. D. LaCount and J. Jaworska, *J. Pharm. Sci.*, 2019, **108**, 337–349.

48 E. B. Souto, J. F. Fangueiro, A. R. Fernandes, A. Cano, E. Sanchez-Lopez, M. L. Garcia, P. Severino, M. O. Paganelli, M. V. Chaud and A. M. Silva, *Heliyon*, 2022, **8**, e08938.

49 E. Caffarel-Salvador, M. C. Kearney, R. Mairs, L. Gallo, S. A. Stewart, A. J. Brady and R. F. Donnelly, *Pharmaceutics*, 2015, **7**, 397–412.

50 R. F. Donnelly, T. R. R. Singh, M. J. Garland, K. Migalska, R. Majithiya, C. M. McCrudden, P. L. Kole, T. M. T. Mahmood, H. O. McCarthy and A. D. Woolfson, *Adv. Funct. Mater.*, 2012, **22**, 4879–4890.

51 A. Ramalheiro, J. L. Paris, B. F. B. Silva and L. R. Pires, *Int. J. Pharm.*, 2020, **591**, 119942.

52 M. J. Garland, K. Migalska, T. M. Tuan-Mahmood, T. R. R. Singh, R. Majithija, E. Caffarel-Salvador, C. M. McCrudden, H. O. McCarthy, A. D. Woolfson and R. F. Donnelly, *Int. J. Pharm.*, 2012, **434**, 80–89.

53 Y. L. Jeyachandran, E. Mielczarski, B. Rai and J. A. Mielczarski, *Langmuir*, 2009, **25**, 11614–11620.

54 I. C. Lee, J. S. He, M. T. Tsai and K. C. Lin, *J. Mater. Chem. B*, 2015, **3**, 276–285.